5
In-situ hydrothermal sensitization of Mesoporous electrode

5.1 Introduction

Several process parameters play important role in the photovoltaic performance of prepared Quantum Dot Sensitized Solar Cells. Sensitization of mesoporous electrode is one of the most important process parameter that governs the performance of final QDSSC. A sensitization scheme governs the mode of attachment of quantum dots to mesoporous electrodes, size of attached quantum dots, capping ligand attached to electron transport material and semiconductor QDs loading fraction. A sensitization scheme should ideally offer monolayer covering and significant loading with precise control of size and shape of quantum dots in direct mode of attachment with electron transport material, as discussed in section 2.2.3. Various sensitization schemes have been adopted in past, but none of them exactly fulfills the desired needs.

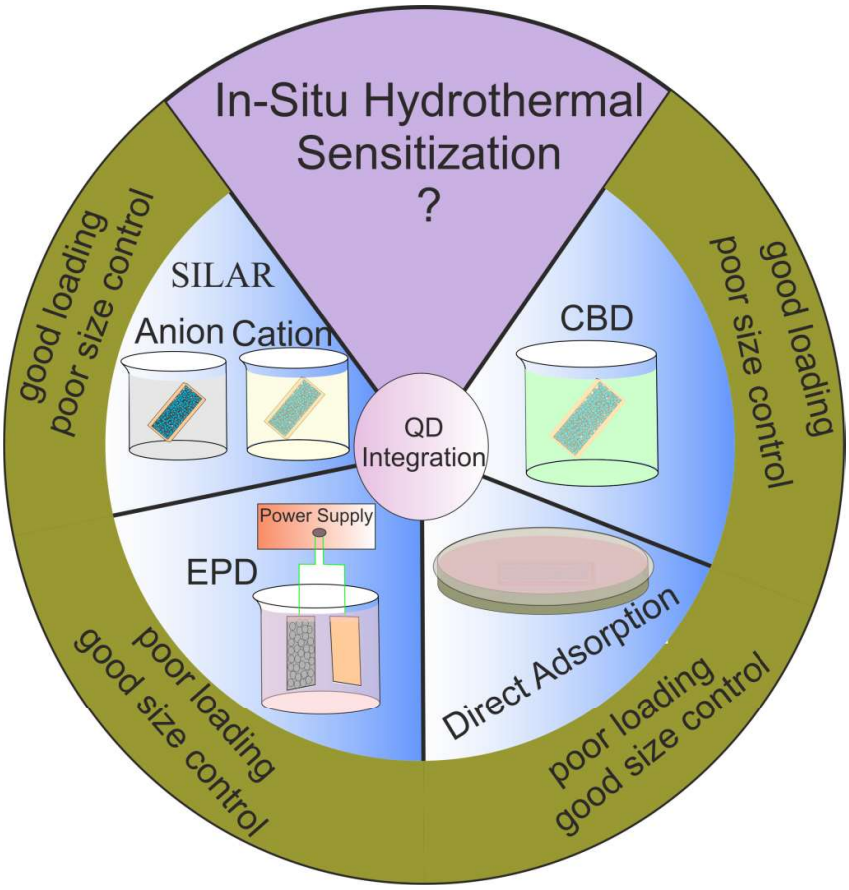

Figure: 5.1 Schematic diagram explaining different sensitization schemes adopted in past.

Figure 5.1 summarize major sensitization approaches adopted by various researchers in past and their pros and cons. Each of these sensitization scheme offer different way of QDs' loading, mode of attachment and control of optoelectronic properties of quantum dots during sensitization. Successive Ionic layer Adsorption and Reaction (SILAR) is one of the oldest and very fast sensitization schemes for mesoporous electrodes. This scheme is discussed earlier in section 4.1.3.2. This sensitization scheme offers good quantum dots loading but control of optoelectronic properties or control of size, shape and composition of quantum dots is a challenge. Number of SILAR cycles is an important sensitization parameter and usually investigated to find an optimized number of SILAR cycles for efficient working device [Lai et al., 2012] but still this is very far from ideal sensitization scheme. Chemical Bath deposition (CBD) is also one of the widely adopted sensitization schemes. In this sensitization scheme, both cationic and anionic precursors are dissolved separately in suitable solvent and later on both precursor solutions are mixed together. Mesoporous electrodes are dipped in ionic mixture and ionic precursors react slowly, resulting in quantum dots deposition over electrode surface. Dipping time and chemical bath conditions are the controlling parameters for QDs growth and coverage [Lai et al., 2012]. Post synthesis sensitization schemes like electrophoretic deposition [Salant et al., 2010], direct adsorption and linker assisted direct adsorption [Pernik et al., 2011] have been also utilized in past. In electrophoretic deposition, large electric field is applied between electrodes to deposit charged QDs over mesoporous electrode. In this sensitization scheme, optoelectronic properties are preserved but obtaining a good surface coverage is a challenge. In direct adsorption, mesoporous electrodes are dipped in dispersed solution of QDs and QDs get deposited in mesoporous electrode. While mode of attachment is direct in nature but achieving good surface coverage is a challenge. Linker assisted direct adsorption is similar to the direct adsorption, but mesoporous electrode is treated with a linker molecule before it is dipped in QDs dispersion solution.

This work focuses on in-situ hydrothermal sensitization of CdTe QDs inside mesoporous electrode. CdTe Quantum dots attachment to mesoporous electrode and photovoltaic properties of sensitized electrodes are investigated. It is found that in-situ hydrothermal sensitization results in a comparatively more efficient CdTe QDSSC as compared to other CdTe based QDSSCs [Bang and Kamat, 2009], [X. Shen et al., 2015]. CdTe QDs are reported to be unstable in polysulfide electrolyte; hence in past they have shown poor photovoltaic response. However in this case, we have found that an amorphous coating is present over sensitized mesoporous electrode that works as a protective layer and relatively good photovoltaic response is obtained.

5.2 Experimental Procedure

Experimental procedure for preparation of in-situ hydrothermal sensitized electrodes and assembling of QDSSCs is discussed in following subsections.

5.2.1 Mesoporous Electrode Preparation

Anatase titanium oxide nano particles have been utilized as a photoelectrode material in this study. FTO substrates were cleaned as discussed in section 4.1.1.1. Cleaned FTO substrates were treated with $TiCl_4$ as discussed in section 4.1.1.2. A paste was prepared as discussed in section 4.1.2.2 for Dr. blade deposition. The prepared paste was deposited on treated FTO substrate using Dr. blade method and electrodes were dried and sintered as discussed in section 4.1.2.3. The prepared mesoporous electrodes are either used directly or stored in vacuum for later use.

5.2.2 Mesoporous Electrode Sensitization and Surface Treatment

Mesoporous electrode has been sensitized using in-situ hydrothermal sensitizations scheme as discussed in section 4.1.3.1. This sensitized mesoporous electrode has been treated with ZnS as discussed in section 4.1.3.3.

5.2.3 Quantum Dot Sensitized Solar Cell Preparation

Assembling of quantum dot sensitized solar cell and testing have been discussed in section 4.1.6. Polysulfide electrolyte preparation details have been discussed in section 4.1.4 and polysulfide electrolyte insertion has been discussed in section 4.1.6. The schematic process flow for in-situ sensitization and photovoltaic characterization are shown in Figure 5.2.

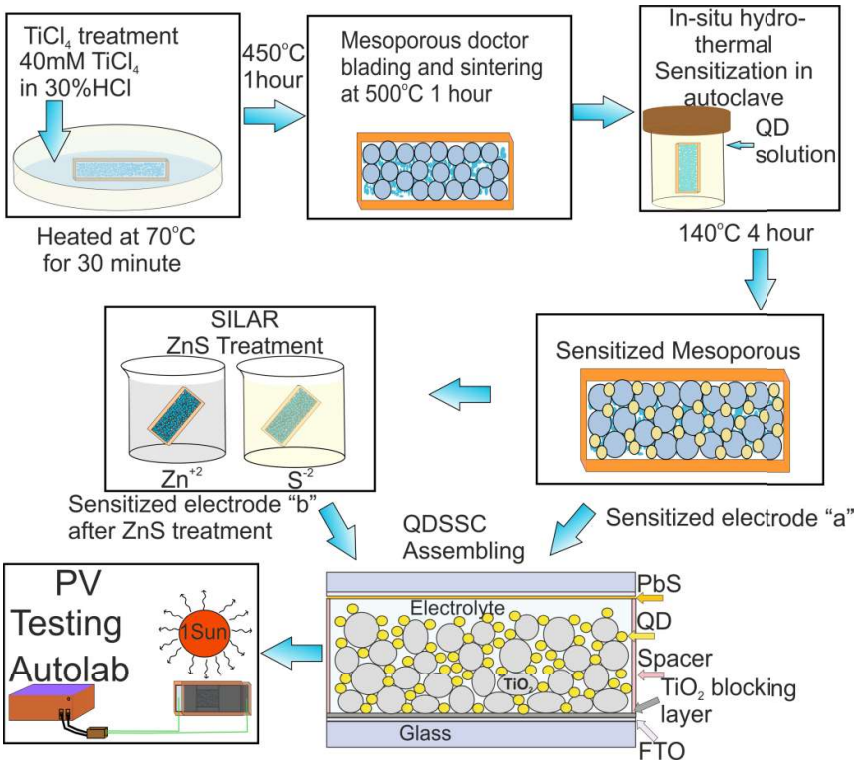

Figure: 5.2 Schematic diagram showing process flow for experimental procedures for in-situ sensitization and PV testing.

5.2.4 Mesoporous Electrode and Sensitized Mesoporous Electrode Characterization

Structural characterization of sensitized mesoporous and pristine mesoporous electrode has been done using X-ray diffraction as discussed in section 4.2.1.1. Surface morphology of sensitized and pristine mesoporous electrode has been studied using scanning electron microscopy as discussed in section 4.2.1.2. Topography of sensitized and pristine mesoporous electrode has been done using AFM as discussed in section 4.2.1.3 in non-contact mode. JEOL JEM-2100 transmission electron microscope was utilized for imaging sensitized mesoporous electrode using copper grid as discussed in section 4.2.2.4. The diffuse reflectance measurements were carried out over sensitized and pristine electrode using DRA accessory as discussed in section 4.2.2.1. The absorbance and emission spectra of prepared QDs were recorded using UV-Vis and Perkin Elmer Fluorescence spectrometer as discussed in section 4.2.2.1 and 4.2.2.3 respectively.

5.3 Results and Discussion

5.3.1 X-ray Diffraction Analysis

X-Ray diffraction pattern is plotted in Figure 5.3 for quantum dot sensitized mesoporous electrode. A diffraction pattern is plotted along with ICDD # 01-089-3011 for anatase titanium dioxide diffraction pattern in upper panel of Figure 5.3. Diffraction peak positions at 26.40°, 33.60°, 51.56°, 61.70° and 65.10° correspond to FTO substrate [Tachan et al., 2010] and marked with the square symbol. The grain size of anatase particles were calculated using Scherrer formula and found to be 34±2 nm [Monshi et al., 2012]. The X-ray diffraction pattern was matched with ICDD 01-075-2083 and a low intensity diffraction peak at 27.7° 2 θ is marked for (200) plane for CdTe QDs.

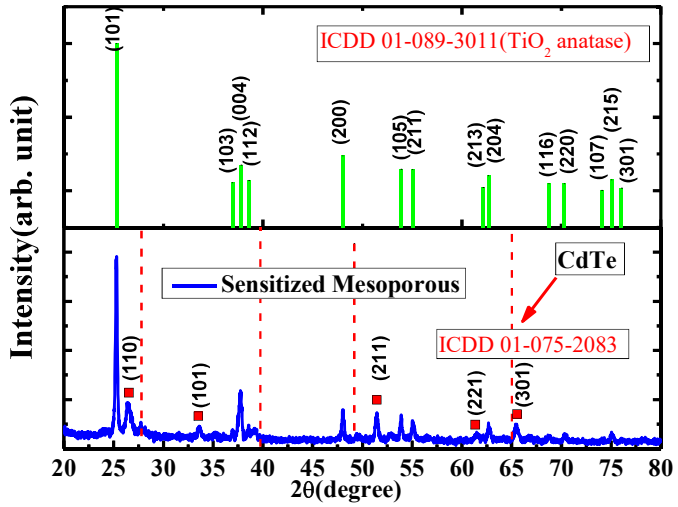

Figure: 5.3 X-ray diffraction pattern for sensitized mesoporous electrode

5.3.2 Microstructure and Surface roughness analysis

Surface morphology of sintered and sensitized electrode was collected to understand microstructure and is shown in Figure 5.4. Low magnification images are shown, in Figure 5.4 (a) and Figure 5.4 (b) for sintered and sensitized electrodes. We can see presence of some aggregates over surface of mesoporous electrode after sensitization. Figure 5.4 (c) shows high magnification image of sensitized electrode, where pores and particle interconnection is visible clearly. Figure 5.4 (d) shows cross sectional image of sensitized electrode and thickness of electrode is found to be 15.23±0.33 μm.

Elemental Dispersive X-ray (EDX) accessory with a SEM system was used to perform Cd/Te quantization inside mesoporous electrode. We got signal for CdTe within error limit of EDS or EDX system and this poor signal can be attributed to the lower weight percentage of CdTe in mesoporous electrode. Scotch tape was used to peel off successive layer of sensitized electrode to investigate qualitatively penetration of QDs inside mesoporous electrode. We got uniform color distribution throughout the thickness of mesoporous electrode, suggesting effective penetration of QDs inside mesoporous electrode.

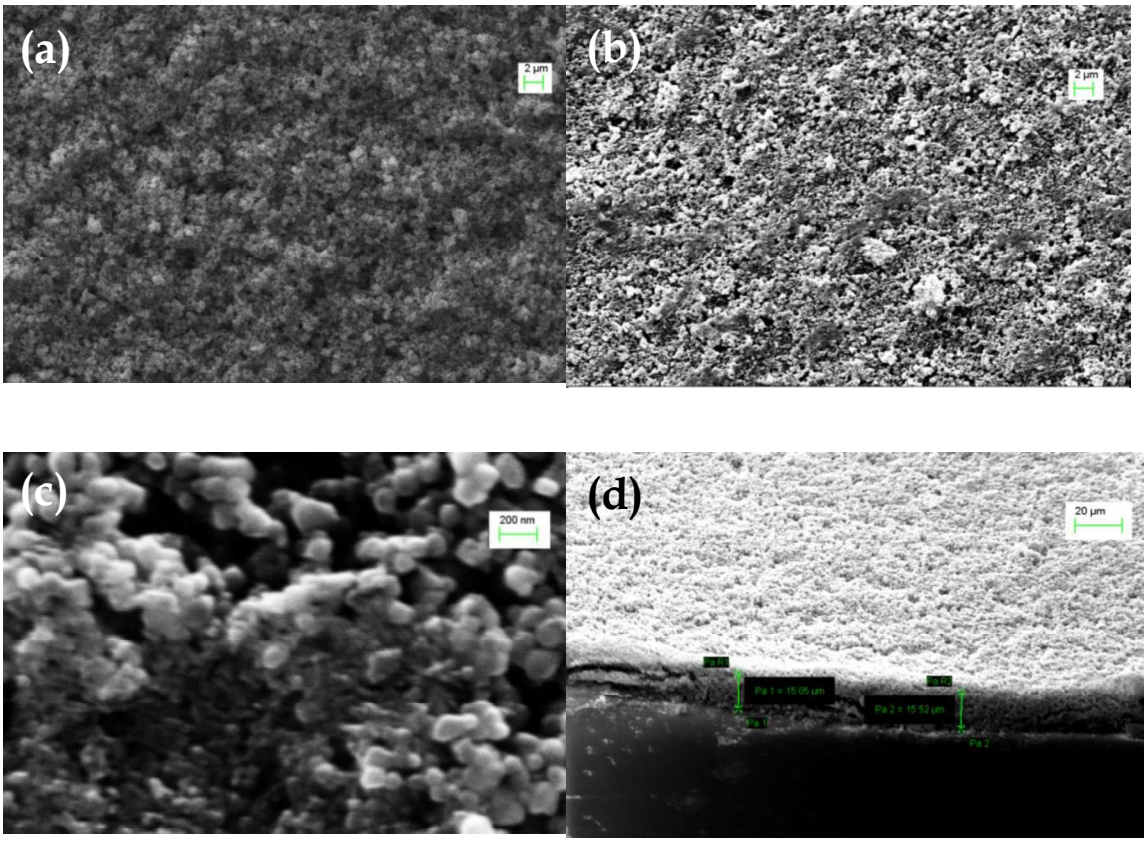

Figure: 5.4 Surface morphology of (a) sintered, (b) sensitized, (c) magnified sensitized mesoporous electrode and (d) cross section of mesoporous electrode.

Topographical differences were investigated in pristine and sensitized electrode using atomic force microscopy. Figure 5.5 shows AFM topographs for 20 µm × 20 µm, 10 µm × 10 µm, 5 µm × 5 µm scan area in Figure 5.5(a, d), Figure 5.5(b, e) and in Figure 5.5(c, f) respectively. Surface roughness (Rq) was calculated for both cases and shown in Figure 5.5.

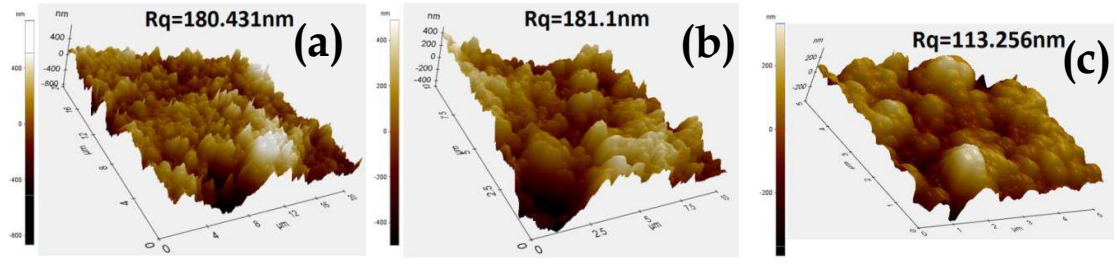

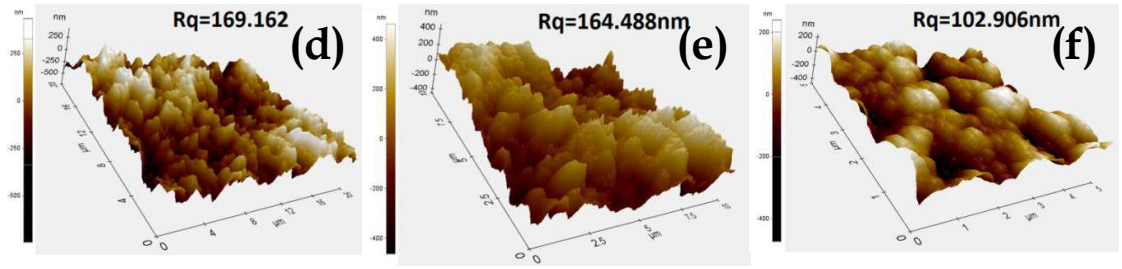

Figure: 5.5 AFM topo-graphs for (a, b, c) sintered and (c, d, e) sensitized electrodes for different scanning area.

AFM topographs for 1 µm × 1 µm scan area is shown in Figure 5.6(a) for CdTe QDs sensitized electrode and Figure 5.6(b) shows pristine electrode. Pattern in Figure 5.6(a) shows smaller QDs in contact of bigger particles of TiO_2. Size of smaller size entities is less than 10 nm. Larger size of QDs can be attributed to size broadening due to the resolution limitation and aggregation of QDs. Effective mass calculations are discussed in section 5.3.4 and estimated size of QDs was found to be ~5 nm.

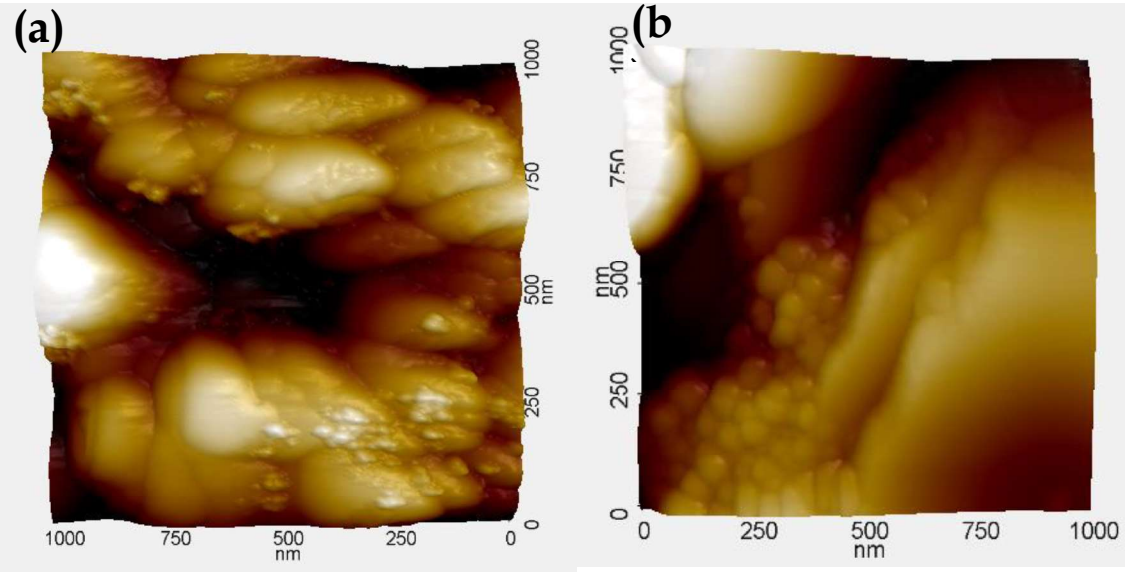

Figure: 5.6 AFM topo-graphs for (a) sensitized and (b) sintered mesoporous electrode for 1 µm × 1 µm scan area.

5.3.3 HR-TEM Analysis of Sensitized Mesoporous Electrode

HRTEM was used to analyze intra structure of sensitized mesoporous electrodes. Sensitized mesoporous electrodes were crushed and dissolved and deposited over Cu grid. A HRTEM image is shown in Figure 5.7 for sensitized mesoporous electrode. CdTe QDs (in red circle), indicated by its characteristic d-spacing is marked in the respective figure. Size of CdTe QDs identified by its characteristic d-spacing in respective insert is about ~5 nm in agreement to size predicted by effective mass calculation. The fringes indicated by the red circled region, shown in Figure 5.7(b), has been used to estimate the d-spacing of CdTe quantum dots using Image J software and found to be 1.936 Å ± 0.035 Å [Abràmoff et al., 2004]. This spacing

corresponds to (121) tetragonal CdTe plane, in agreement with CdTe ICDD database file 03-065-7967 reference. The accuracy of CdTe QDs d-space measurements is confirmed by cross validating with the internal known fringes of the (101) anatase TiO_2 plane with the reference ICDD database file 03-065-5714. For (101) anatase TiO_2, we got d-space of 3.584 ± 0.022 Å which is deviated by 2 % from the tabulated PDF. These measurements were calibrated against TiO_2 anatase phase, which has been used as internal standard for these calculations. HRTEM images also indicate the additional amorphous coating on sensitized electrodes of ~ 3 nm, as shown in Figure 5.7(a). This coating is attributed to the excess NAC used during the mixing of precursors.

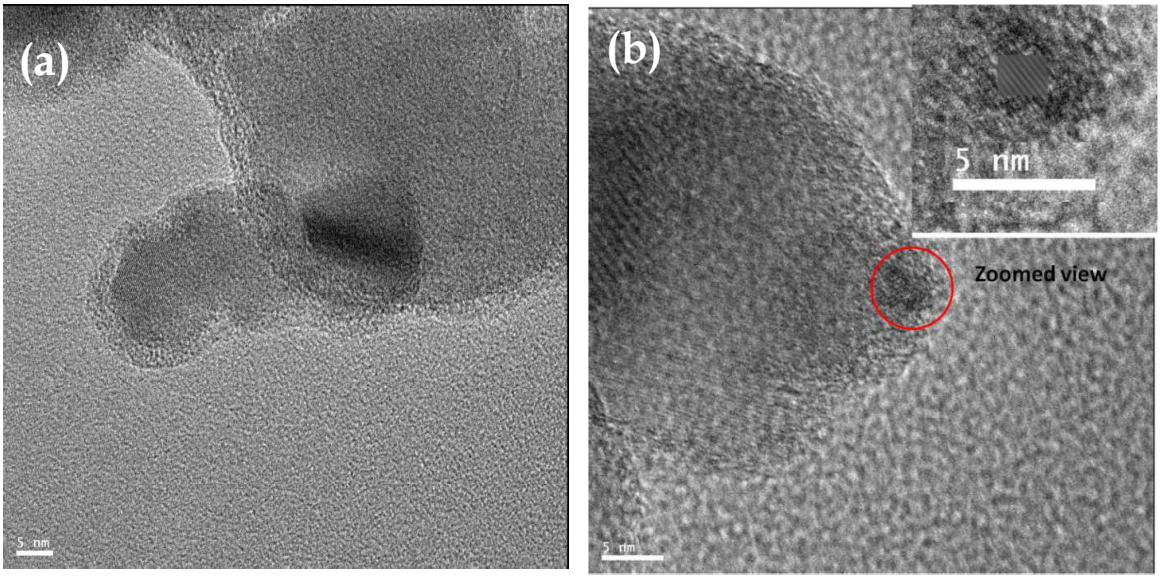

Figure: 5.7 HR-TEM image for sensitized mesoporous electrode (a) Image showing organic covering and (b) d-spacing calculation for CdTe quantum dots.

5.3.4 Optical Characterization

UV-Vis and fluorescence spectrometers were used to measure absorbance and emission spectra of CdTe QDs dispersed in DI water. Optical absorbance onset was estimated to be 600±5 nm while emission corresponds to 607±5 nm. Bandgap of CdTe from emission measurement was calculated from effective mass approximation [Pejova and Grozdanov, 2005] equation

$$R = \frac{-0.3649 + \sqrt{0.1331 + 17.864 * \Delta E_g}}{2 * \Delta E_g}$$

where R is radius of quantum dots and ΔEg (in eV) is the difference in the electronic bandgap of bulk CdTe and CdTe quantum dots. The calculated bandgap from emission is 2.04±0.15 eV and estimated size from effective mass approximation is 5.11±0.06 nm. This size is consistent with TEM measurements.

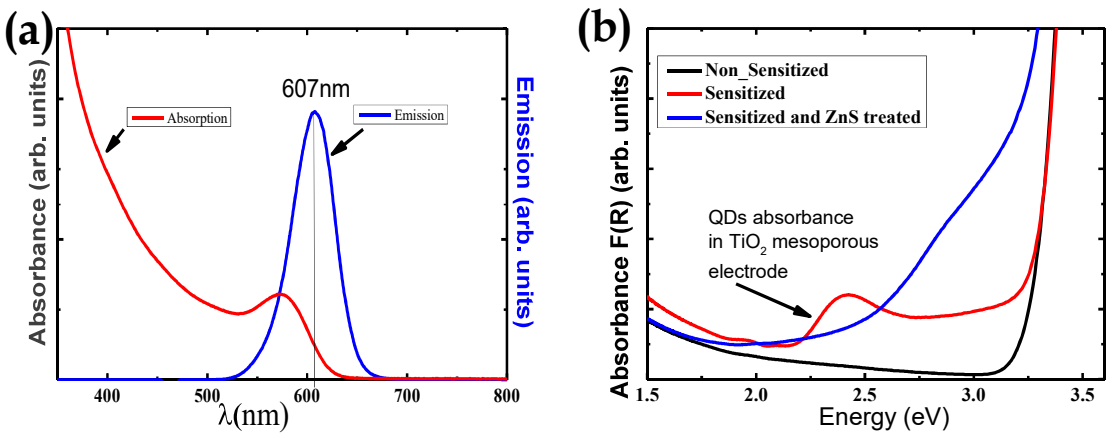

Figure: 5.8 (a) absorption and emission spectra of dispersed QDs and (b) Absorbance calculated from diffuse reflectance measurement for sensitized, non-sensitized and ZnS treated electrode.

Diffuse reflectance measurements were done on sintered mesoporous electrode and sensitized mesoporous electrode before and after ZnS treatment. Kubelka-Munk model [Džimbeg-malčić et al., 2012] is used to calculate the absorbance using diffuse reflectance data and results are plotted in Figure 5.8(b). Absorbance of CdTe quantum dots was found to be at 2.2 eV showing that CdTe QDs were integrated in TiO_2 mesoporous electrodes. This absorbance become less prominent for ZnS treated electrode and peak broadening is attributed to additional wider bandgap ZnS protective layer growth on CdTe quantum dots. Impact of this layer is discussed in photovoltaic characterization section.

5.3.5 Photovoltaic Characterization

Photovoltaic properties of sensitized electrode were evaluated in 2 electrode configuration under 1 Sun intensity illumination. Recorded photovoltaic performance is shown in Figure 5.9. Photovoltaic response without any additional surface treatment (case "a") and with ZnS surface treatment (case "b") is shown in Figure 5.9.

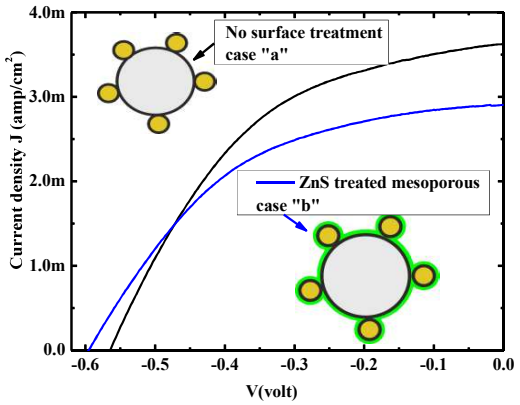

Figure: 5.9 Photovoltaic response of sensitized electrode with and without ZnS treatment under 1 sun intensity illumination.

Photovoltaic performance parameters were extracted from recorded I-V response and summarized in table 5.1. 4 devices were prepared and variation among devices is shown in

table with standard deviation. Normally, after ZnS surface passivation I-V response improves [Néstor Guijarro et al., 2011] but in this case we got better photovoltaic response without any additional surface passivation. These in-situ hydrothermal sensitized electrodes were stable under polysulfide electrolyte [Bang and Kamat, 2009]. In present work, the observed NAC organic layer covering, discussed in section 5.3.3, works as protective covering for CdTe QDs, which are known to be unstable in polysulfide electrolyte.

Table 5.1 Photovoltaic response parameters for CdTe sensitized electrodes with and without ZnS treatment.

S. No.	Electrode Specifications	J_{sc} (mA/cm^2)	V_{oc} (Volt)	FF	Efficiency (%)
1	$TiCl_4/TiO_2$/ CdTe/ PbS	3.35 ± 0.21	0.58 ± 0.01	49 ± 3	0.95 ± 0.04
2	$TiCl_4/TiO_2$/CdTe/ZnS/PbS	2.78 ± 0.19	0.62 ± 0.01	47 ± 2	0.78 ± 0.02

Normally ZnS protective covering enhances the photovoltaic performance of CdTe based QDSSCs. This layer normally provides the surface passivation of CdTe QDs, which helps in reducing back recombinations. But as per observations, in-situ hydrothermally sensitized electrodes do not require any additional surface passivation. Further, we also carried out ZnS surface passivation on these in-situ CdTe QDs sensitized mesoporous electrodes and improvement in open circuit voltage is observed after ZnS treatment, indicating the reduced back recombination but reduction in photocurrent is observed simultaneously. This reduction in photocurrent is attributed to the combined effect of ZnS surface passivation layer and amorphous organic protective covering.

Impedance spectroscopy was utilized to probe further differences in sensitized electrode with and without ZnS surface passivation. Impedance measurements were performed on fabricated QDSSCs at different forward bias voltage (0 Volt - V_{oc}) for 100 kHz to 0.1 Hz frequency range with 10 mV ac voltage under dark condition. The measured impedance data is fitted using equivalent circuit model discussed under section 4.2.3.2. Recorded Nyquist plots are shown in Figure 5.10 along with equivalent circuit fitted data.

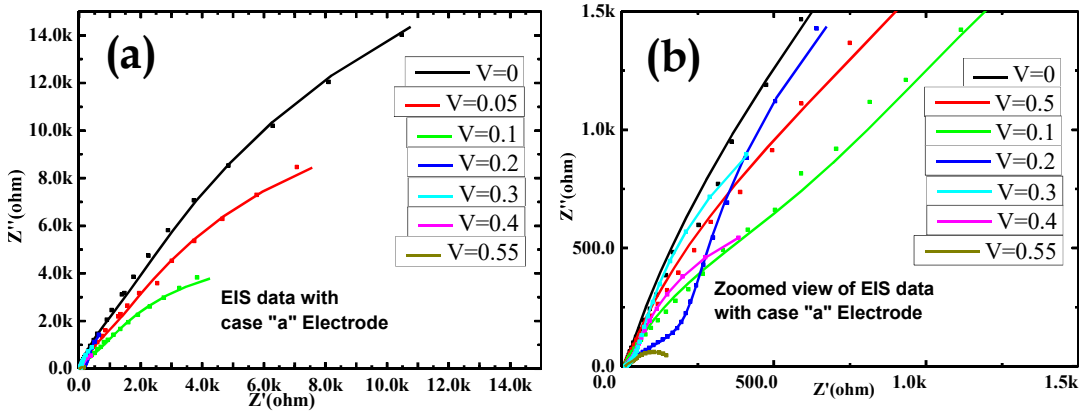

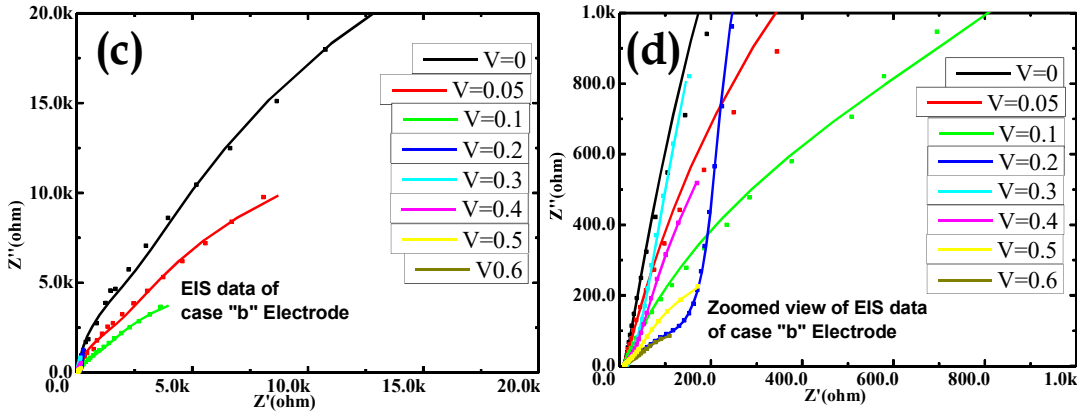

Figure: 5.10 Nyquist plots for (a, b) Without ZnS treatment sensitized electrodes and (c, d) with ZnS treatment under different bias conditions.

Extracted interfacial resistances and capacitances after fitting with equivalent circuit models are plotted in Figure 5.11. It was observed that measured series resistance is similar to reported literature [X. Shen et al., 2015]. We have observed that transport resistance has increased after ZnS surface treatment, suggesting the presence of an additional barrier in electron transport. A plateau in chemical capacitance is observed at intermediate potential range 0.4 V, that is related to deep surface states of TiO_2 consistent with earlier reported observation in literature [Mora-Seró et al., 2009]. These measurements suggest no significant change in counter electrode resistance for both cases since similar counter electrode material and electrolyte were utilized for both devices. Impedance data showed poor Kramers - Kronig fits for potential below 0.2 V, suggesting poor reliability of the simulated results. So parameters below 0.2 V were not used in discussion.

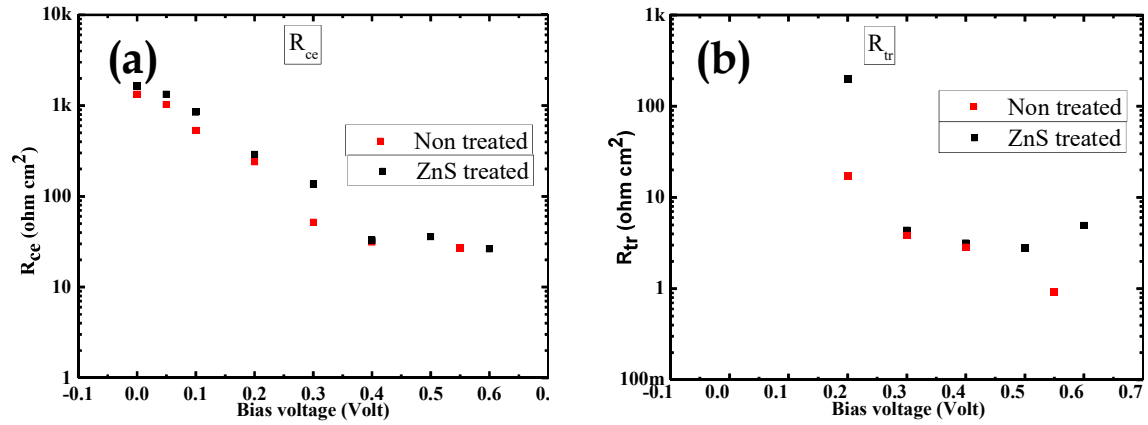

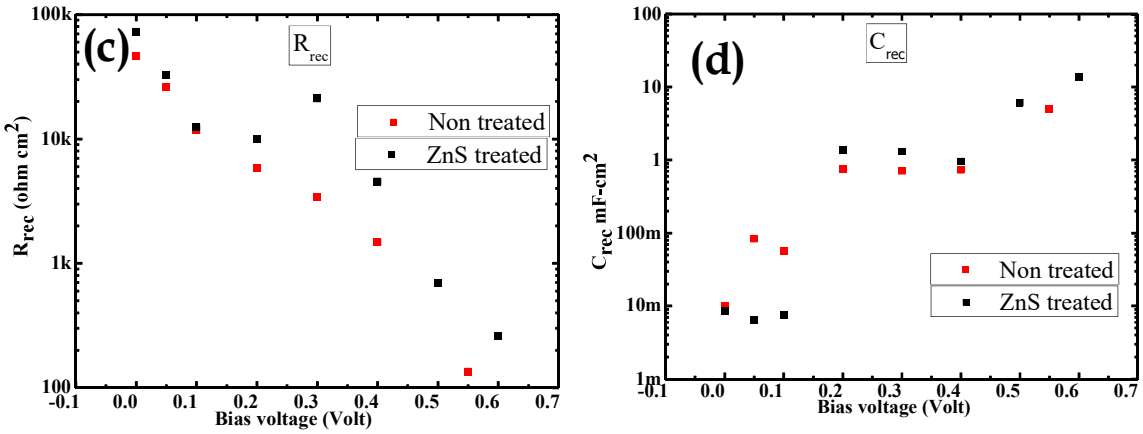

Figure: 5.11 Extracted parameter from impedance data fitted with equivalent circuit models (a) Counter electrode resistance R_{ce}, (b) transport resistance R_{tr}, (c) recombination resistance R_{rec} and (d) recombination capacitance C_{rec}.

5.4 Concluding Remarks

An in-situ hydrothermal sensitization process was adopted for integration of CdTe QDs in TiO_2 mesoporous electrode. This process resulted in superior photovoltaic performance without the requirement of additional surface passivation. HRTEM images suggested the presence of an amorphous organic protective covering that protect CdTe quantum dots from polysulfide electrolyte. These prepared sensitized mesoporous electrodes showed better photovoltaic performance compared to recent anion exchange CdTe integrated mesoporous electrodes. Short circuit current density of 3.35±0.21 mA/cm^2 was obtained that is the best among CdTe based devices. Further ZnS passivation resulted in decrement of current density suggesting that sensitized electrodes do not require further passivation.

...